RSC Advances

ROYAL SOCIETY OF CHEMISTRY

www.rsc.org/advances

RSC Advances

RSCPublishing

ARTICLE

Adsorption, photodegradation and antibacterial study of Graphene-Fe_3O_4nanocomposite for multipurpose water purification application

Cite this: DOI: 10.1039/x0xx00000x

Received 00th January 2014,
Accepted 00th January 2014

DOI: 10.1039/x0xx00000x

www.rsc.org/

Chella Santhosh[a], Pratap Kollu[b*],Sejal Doshi[c], Madhulika Sharma[c], Dhirendra Bahadur[c*], Mudaliar Vanchinathan.T[a], P.Saravanan[d], Byeong-Su Kim[e]and Andrews Nirmala Grace[a*]

Graphene-Fe_3O_4 (G-Fe_3O_4) composite was prepared from graphene oxide (GO) and $FeCl_3.6H_2O$ by one step solvothermal route. The as-prepared composite was characterized by Field emission-Scanning electron microscope, Transmission electron microscope, Dynamic light scattering (DLS) and X-ray powder diffraction. SEM analysis shows the presence of Fe_3O_4 spheres with size ranging between200-250nm, distributed and firmly anchored onto the wrinkled graphene layers with a high density. The resulting G-Fe_3O_4 composite shows extraordinary adsorption capacity and fast adsorption rates for removal of Pb metal ions and organic dyes from aqueous solution. The adsorption isotherm and thermodynamics were investigated in detail and results show that the adsorption data was best fitted with the Langmuir adsorption isotherm model. From the thermodynamic investigation, it was found that the adsorption process is spontaneous and endothermic in nature. Thus, the as-prepared composite can be effectively utilized in the removal of various heavy metal ions and organic dyes. Simultaneously, photodegradation of methylene blue was studied and the recycling degradation capacity of dye by G-Fe_3O_4 wasanalyzed upto 5 cycles, which remained consistent to ~97% degradation of methylene blue dye. Though iron oxide has affinity towards bacterial cells, still its composite with graphene has shown antibacterial property. Almost 99.56% cells were viable when treated with Fe_3O_4 nanoparticles treatment whereas with the composite, barely 3% cells survived. Later on, release of ROS was also investigated by membrane and oxidative stress assay. Total protein degradation was analyzed to confirm the effect of G-Fe_3O_4composite on *E.coli* cells.

Introduction

Water pollution due to biotic and abiotic pollutants has been a major environmental threat due to existing and emerging industries. Heavy metals and dyes beyond the permissible limits cause toxicity directly to humans and other living organisms. Metal ions such as cadmium (II), Pb (II), and chromium (II) have been found to be effective in immobilizing the enzyme by attacking sulphur in some plants and some of the metal ions are so toxic that it can cause energy deficiency in the transmission of nerve impulse in humans[1, 2]. Hence, it has been need of the hour to prevent water pollution caused due to microbes as well as heavy metals and dyes. Most of the purification methods suffer from some drawbacks, such as high capital and operational cost or disposal of residual metal sludge and are not suitable for small scale industries[3]. These methods are not much efficient at low concentration in the range of 1 to 100 mg/L[4,5]. Silver has laid the foundation of antibacterial activity. But, as silver is expensive and leaches into the environment, the focus has been shifted to explore inexpensive materials for antibacterial activity.

Adsorption is one of the promising processes for removal of heavy metal ions from water. Some of the adsorbent material for heavy metal ion removal are activated carbon (powder or granular), CNTs, etc[6-8] for the removal of Pb, cadmium and other heavy metal ions. However, the cost of the adsorbent becomes relatively high when pure sorbents are used. Similarly photodegradation of the dye has been a successful methodology to eradicate dyes from effluent water, thus helping further in water purification.

Graphene and Fe_3O_4[9,10] individually have been reported for their filtration and purification activity. As a stand-alone they draw a potential of being used as a water purifying material, thus it was thoughtful to combine them as a composite and efficiently use it as a combine nanomaterial for water purification. Graphene is a single layer of carbon densely packed in a honey comb crystal lattice structure. In comparison with other carbonaceous material, it has drawn much attention since its discovery due to its unique electronic and mechanical properties[11,12]. Its remarkable properties such as huge surface areas (2630 m^2/g), good chemical stability, flat structure, can be used as an excellent adsorbent [13-16]. The basal plane structure allow it to have strong π-π interactions, assigned to the π-π stacking between aromatic dyes and π-conjugation regions of the graphene layers[17].This property of graphene would serve as a good adsorbent for removing pollutants such as metal ions, dyes, and biological applications. Graphene sheets usually suffer from serious agglomeration and restacking, due to their π-π interactions between neighbouring sheets, leading to a great loss of effective surface area and lower adsorption capacity[18,19]. To overcome such difficulties, magnetic adsorbent have emerged as a new generation material for environmental applications. The advantages of such materials are magnetic separation by applying external magnetic field to extract the adsorbent material from the suspension[20, 21].

Compared with the traditional methods such as filtration, centrifugation, gravitational separation, the magnetic separation requires less energy and better separation can be achieved. Therefore, synthesis of graphene with covalently attached Fe_3O_4 offers an effective approach to overcome the separation problem associated with graphene. At the same time, the attachment of Fe_3O_4 to graphene provides decrease in possibility of serious agglomeration. In this regard, this work is focused on the synthesis of G-Fe_3O_4 composites by solvothermal route. Further, the as-prepared composite were tested for its adsorption property towards Pb ions and photodegradation of methylene blue was also performed. To better understand its antimicrobial mechanism, we compared the antibacterial activity of graphene and G-Fe_3O_4 towards a bacterial model; Escherichia coli. Under similar concentration and incubation conditions, G-Fe_3O_4 dispersion shows the highest antibacterial activity. ROS[22]and protein degradation were responsible for bacterial cell wall rupture.

Experimental

Materials

All the chemicals were analytical grade, purchased from Sigma Aldrich and used as received without purification. Graphite powder, hydrogen peroxide (30 wt %), sodium nitrate (98%), sulphuric acid (98 wt%), potassium permanganate,$Pb(NO_3)_2$, $FeCl_3.6H_2O$ and sodium acetate (NaAc) were purchased from SD-Fine and were used as received.

Preparation of graphene oxide

Graphene oxide (GO) was prepared from natural graphite powder by modified Hummers method.[23]In a typical synthesis, 1 gm of graphite was added into 23 ml of 98% H_2SO_4, followed by stirring at room temperature over a period of 24 hrs. Then 100 mg of $NaNO_3$ was added into the mixture and stirred for 30 min. Subsequently, the mixture was kept below 5^{o}C in an ice bath, and finally, 3 gm of $KMnO_4$ was added slowly into the mixture. Afterwards, the mixture was heated to 35-40^{o}C with continuous stirring for 30 min. Then 46 ml of water was added into the above mixture and mixed well for 25 min. Finally, 140 ml of water and 10 ml of 30% H_2O_2 were added into the mixture to stop the reaction. After this, unexploited graphite in the resulting mixture was removed by centrifugation; the resulting mixture was dried at 60^{o}C in a vacuum oven. The as-synthesized GO was dispersed into individual sheets in distilled water at a concentration of 0.5 mg/mL with the aid of ultrasound for further use.

Synthesis of G-Fe_3O_4nanocomposites

The above prepared GO was used as a precursor for the preparation of G-Fe_3O_4 composites by one step solvothermal method. In a typical synthesis, the as-prepared GO (0.5g) was exfoliated by ultrasonication in 80 mL of ethylene glycol for more than 3 h. 1.6 g $FeCl_3 \cdot 6H_2O$ and 3.2g NaAc were then dissolved in GO/EG solution at ambient temperature. After stirring for about 30 min, the solution was transferred to a 100 mL Teflon-lined stainless-steel autoclave and kept at 200^{o}C for 6 h followed by cooling to ambient temperature naturally. The black precipitate was centrifuged, washed with ethanol several times, and finally dried at 60^{o}C in a vacuum oven.

Characterization

The particle size and morphology of the material was studied by FE-Scanning Electron Microscopy (FE-SEM) (HITACHI SU6600 SEM). The phase and the crystallographic structure were identified by X-ray diffraction (XRD, Philips X' Pert Pro, Cu-Kα: λ=0.1540598 nm). The metal ion concentration adsorbed by the adsorbent was examined by atomic adsorption spectrophotometer (Perkin-Elmer Analyst 240). Thermogravimetric analysis (TGA) of the samples was done with a SDT Q600 (TA Instruments, Korea) with a heating rate of 5°C min^{-1} from 0° to 1000°C. The G-Fe_3O_4 samples were characterized with high resolution Transmission Electron Microscope (HR-TEM) JEOL-2000EX operated at 120 kV. Dynamic light scattering measurements were done using

Analytical measurement

For analytical studies lead nitrate of analytical grade was used to prepare a stock solution, containing 1000 mg/L of $Pb(NO_3)_2$,which was further diluted with double distilled deionized water to the required ion concentration. Adsorption thermodynamics experiments were conducted in a 100 ml glass flask containing 25 mg of adsorbent and 100 ml of Pb ion solution containing varying concentrations (10-50 mg/L) at pH 5. The samples were then placed in an orbital shaker for continuous stirring at 250 rpm for different period of time and at various temperatures (300, 310, and 320 K). After a certain time, the suspension was filtered using 0.22 µm cellulose nitrate membrane then, the filtrates were immediately examined using atomic adsorption spectrophotometry (AAS) in order to measure the ion concentration. The difference between the initial and the equilibrium ion concentration gives the amount of ion adsorbed onto the G-Fe_3O_4surfaces.

Batch mode adsorption

The effect of experimental parameters, such as initial concentration (10-50 mg/L), pH (3-8), and temperature were studied in a batch mode of adsorption for specific period of contact times (0-180 min). In order to determine the effect of each parameter, the other parameters were fixed. Pb solution was prepared by dissolving $Pb(NO_3)_2$ in double distilled water and used as stock solution. Then, they were diluted to the required concentration for the experimental study. The pH of the solution was adjusted using 0.1 M HCl or 0.1 M NaOH. For contact time measurements, 100 ml of Pb ion solution containing 10 mg/L of initial ion concentration at pH 5 was taken in a 250 ml conical flask with a fixed quantity of adsorbent (25 mg/L) and agitated in an orbital shaker at 250 rpm and 310 K. At various intervals, the adsorbent were separated from the samples by filtering and the filtrates were analyzed using AAS to determine the concentration of each ion in the solution.[24]The adsorption percentage of metal ion was calculated as follows:

$$Adsorption\ (\%) = \frac{C_i - C_f}{C_i} X\,100 \qquad (1)$$

Where C_i and C_f are the initial and final metal ion concentration (after contact to adsorbents) respectively.

Photodegradation activity of G-Fe_3O_4

The photodegradation activity of the as-prepared G-Fe_3O_4 was evaluated by photodegradation of methylene blue dye using 60W of visible light CFL lamp. For the degradation of dye, 0.2g/L of photocatalyst was added to 100 mL of methylene blue dye (10 mg/L) aqueous solution. 1 mL of 30% H_2O_2 was added to the reaction mixture at the beginning of light irradiation. About 1mL aliquot was withdrawn at a given irradiation time and then magnetically separated to remove the catalyst. In the case of bare

graphenenanosheets, the suspension was separated by centrifuging at 3000 rpm. The concentration of the remnant dye was determined by measuring the absorbance of solutions at 664 nm by UV-vis spectroscopy.

Biocompatibility of G-Fe_3O_4

Sulforhodamine-B (SRB) assay was performed to evaluate the biocompatibility of G-Fe_3O_4 with normal mouse fibroblast cells (L929). Though iron oxide nanoparticles have been well established as biocompatible nanomaterial, yet it is essential to evaluate the toxic effect of G-Fe_3O_4 on cell proliferation or morphology of L929 cells due to the presence of graphene. It is important to test the toxic effect of functional material towards a living system. The cells were seeded into 96-well plates at a density of $1x10^4$ cells per well and incubated for 24 h in 5% CO_2 environment. Then, 200 µl of different concentrations of dispersed suspension of G-Fe_3O_4 (2.0, 1.0, 0.5, 0.25, 0.125, 0.625, and 0.3125 mg/ml), in DMEM growth medium, were added to cells and incubated for another 24 h at 37ºC and 5% CO_2 environment. Thereafter, the cells were gently washed with phosphate buffer saline (PBS; pH 7.3) and processed for SRB assay to determine the viable cell population. Non-treated cells were used as control for the experiments. The cells were then fixed with 10% trichloroacetic acid solution by incubating at 4°C for 1 h. This was followed by gentle washing of cells with water and then staining with 0.4% SRB dissolved in 1% acetic acid and then incubating in dark. The cell-bound dye was then extracted with 200 µl of 10 mM Tris buffer solution (pH 10.5) and its optical density was measured using a multiwall plate reader at 560 nm. The viable cell population was calculated using the following formula:

$$\%\ Cell\ Viablity = \frac{Absorbance\ of\ treated\ cells}{Absorbance\ of\ control\ cells} X 100$$

Antibacterial activity of G-Fe_3O_4

E.coli was procured from K.C.College, Mumbai, India. The cultures were initially inoculated from patients infected with water borne disease. This culture has been sub-cultured since last 20 years and hence assumed to have least virulence. Nutrient broth media was procured from Himedia. All chemicals were purchased from Sigma-Aldrich and used without further purification.

Results and discussion

Structural and morphological analysis

The phase composition and structures of G-Fe_3O_4 nanocomposites were examined using X-ray powder diffraction and the corresponding pattern is given in Fig.S1. In the pattern of GO (Fig. S1a), a diffraction peak at 11.08° is observed, which corresponds to the (001) plane of graphene oxide structure. In Fig S1b, natural graphite show diffraction peaks at 26.4°, 44.3° and 54.5° corresponding to the hexagonal lattice of (002), (101) and (004) planes. The major peak is at 26.4° corresponding to a basal spacing d_{002} = 3.38 Å.The typical process is the reduction of GO to graphene during the solvothermal process. After reduction, the peak at 11°totallydisappeared and a weak hump (*) could be observed in Fig S1(c). In Fig S1c, G-Fe_3O_4 composite with diffraction peaks at 2θ values of 30.6°, 36.1°, 43.7°, 57.6°, 63.1° and 74.7°corresponds to (220), (222), (400), (511), (440) and (533) planes of Fe_3O_4 respectively. This matches with the standard JCPDS no. 65-3107. The results indicate the existence of Fe_3O_4 in the composite material and clearly show the reduction of GO peak in the composite material. The disappearance of the peak at 2θ = 11° clearly indicated that GO was reduced to graphene. The absence of sharp peak at 26° indicates that it is not graphite but should be graphene. The peak at 2θ = 26° pertaining to graphene is not so intense, because as it is in the form of composite and the Fe_3O_4 phase dominates the graphene layers. The graphene peak was not predominant as the stacking of graphene sheets in G-Fe_3O_4 was disordered and exfoliated by a large extent[25,26].

Morphological characterization of G-Fe_3O_4

Fig1 shows the surface morphology of G-Fe_3O_4 at various magnifications. The TEM images of G-Fe_3O_4, reveals that the product consists of a large quantity of Fe_3O_4spheres with size ranging from 200-250 nm.After combination with graphene to formG-Fe_3O_4composite, the Fe_3O_4 spheres are decorated and firmly anchored on the wrinkled graphene layers with a high density as shown in Fig. 1. Notably, the pleats structure of graphene may favour to hinder the Fe_3O_4 spheres from agglomeration and enable their good distribution on graphene, while the Fe_3O_4 spheres serve as a stabilizer to separate graphene sheets against aggregation. Also the Fe_3O_4 spheres are observed to be porous in nature, which will further aid the adsorption process.

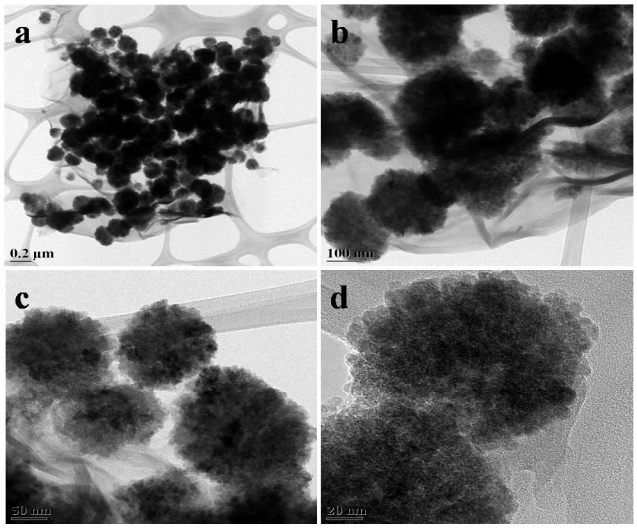

Fig. 1TEM images of G-Fe_3O_4 nanocomposites

Further, dynamic light scattering measurements (DLS) were recorded and results showed that the nanoparticles are monodisperse (Fig.S2a). The hydrodynamic sizes of the particles were found to be around 500 nm. In general hydrodynamic diameter takes into consideration the factors like solvation and other effects and hence will be generally higher than measured by other methods[27]. The sizes of the particles were further confirmed from SEM analysis, which shows the dispersion of Fe_3O_4 particles on graphene sheets (Fig.S2b).

TGA–DTA /BET analysis.

Fig.S3 shows the TGA curve of the as-prepared G-Fe_3O_4 composite with a minor weight loss from 50°C upto 100°C (~10%) and major weight loss from 270°C to 450°C (~40%). After this, no weight loss was obtained up to 1000°C. A minor weight loss observed is due to the adsorbed water and loss of moisture in the as-prepared material. Major weight loss obtained is due to the graphene and Fe_3O_4 composite. Apparently, in DTA curve, two main exothermic peaks

were obtained at 290°C and 450°C, which relates to the thermal decomposition of ferrites along with the carbon compound.

The N_2 adsorption-desorption isotherm was used to determine the porous capacity of Graphene-Fe_3O_4 (Fig. S4a). According to IUPAC (International Union of Pure and Applied Chemistry) classification, the isotherms show the typical type IV and are type H3 hysteresis loop. This behaviour indicates the predominance of mesopores. The mesoporous nature is also evident from the sharp increment in adsorption volume above the relative pressure 0.8. The specific surface area of the composite from BET analysis was found as 27.38 m^2/g. Barrett–Joiner–Halenda (BJH) method was used on desorption branch of N_2 adsorption–desorption isotherm to calculate the pore size. The pore volume versus pore diameter curve (Fig. S4b) shows a sharp peak at 3.7 nm along with broad distribution of mesopores. This behaviour also confirms the predominance of mesopores in G-Fe_3O_4[28].

Adsorption Parameters

To further know the adsorption property of the prepared materials, batch adsorption experiment was run and the corresponding adsorption parameters of lead ions onto G-Fe_3O_4 nanocomposites are shown in the FigS5. Figure S5a shows the removal efficiency of lead ions onto G-Fe_3O_4 surfaces, as a function of contact time. It was noted that the adsorption of Pb increased quickly with an increase in contact time and then at a certain period it reaches an equilibrium state. It was seen that adsorption is fast due to the availability of plenty of active sites on the adsorbent surface at the initial stage. This fast adsorption may be due to the special one-atom-thick layered structure of GO. Also, as it gets in touch with Pb ions in the aqueous solution, the adsorption occurs immediately due to the higher driving force to make transfer of Pb ions faster to the active sites on the surface of G-Fe_3O_4. With further increasing the time, the diminishing availability of the remaining active sites and the decrease in the driving force makes the adsorption process slow and thus equilibrium is achieved much later. Thus, the adsorption rate becomes slower.The equilibrium time increases with increasing initial Pb ions concentration and from the graph (Fig.S5a), it can be concluded that it took about 100 min to reach adsorption equilibrium. From 120-180 min, the concentration of the ions remained unchanged.

Fig. S5b shows the amount of adsorbed ions as a function of the initial concentration from aqueous solution. The initial concentration provides an important driving force to overcome all mass transfer of Pb ions between the aqueous and solid phases, hence a higher initial concentration of Pb ions may increase the adsorption capacity. In this experiment, the following concentration (10, 20, 30, 40, 50 and 60 mg/L) were chosen at pH 5, equilibrium time 120 min and T=310 K. With an increase of ion concentration, the percentage of ion adsorption increased. About 99% of Pb ions were adsorbed onto G-Fe_3O_4 surface after 120 min for the initial Pb concentration of 50 mg/L.Fig.S5c shows the variation of adsorption capacity of Pb ions by G-Fe_3O_4 at various pH values. The adsorption capacity increases with initial pH 3 and reaches a maximum at pH 7. The effect of pH on the adsorption percentage of Pb ions onto the adsorbent G-Fe_3O_4 were studied at varying pH values over the range of 3-8 using the same concentration of ions and the results are given in Fig. S5c. Although a maximum uptake was noted at pH 8, but as the pH increased greater than 7, the metal ion started to precipitate. Therefore, no experiment was conducted at pH >7. The increase in adsorption capacity at pH >7 could be due to both the adsorption of ions onto the surface of adsorbent and precipitation. Therefore, the optimum pH was found to be 5 for the adsorption of Pb ions. By further increase in pH, adsorption decreased probably due to the formation of Pb hydroxides and chemical precipitation.

Fig.S5d shows the adsorption% of Pb ions onto G-Fe_3O_4 matrix as a function of temperature. The percentage of adsorption experiment were conducted at 300, 310 and 320 K to investigate the effect of temperature, with initial concentration of Pb ions being 20 mg/L, adsorbents dosage of 25 mg/L and pH 5. When the temperature was increased from 300 to 320 K, the percentage of adsorption for Pb ions increased from 85.2 to 87.2%. An increase in the amount of equilibrium adsorption of Pb ion with the rise in temperature may be explained by the fact that the adsorbent sites were more active at higher temperature. Thiscondition shows that adsorption occurs more physically rather than chemically.

Adsorption Isotherm study

Developing an appropriate isotherm model for adsorption is essential to design and optimize an adsorption process. Several isotherm models have been developed for evaluating the equilibrium adsorption of compounds from solutions, such as Langmuir,[29,30] Fruendlich and Dubinin-Radushkevich. The experimental results of this study were fitted with the two models. The equilibrium adsorption isotherms are important in determining the adsorption capacity of the Pb ions and diagnose the nature of adsorption onto G-Fe_3O_4 surface.[31]

The equilibrium concentration adsorption capacity of adsorbent was calculated as following equation

$$q_e = \frac{v(C_0 - C_e)}{w} \qquad (2)$$

where q_e is the equilibrium adsorption capacity of adsorbent in mg metal/g adsorbent, C_o is the initial concentration of the metal ions in mgL^{-1}, C_e is the equilibrium concentration of the metal ions in mg/L, V is the volume of metal ion solution in L, and W is the weight of adsorbent in g.

The adsorption data can then be correlated with Langmuir and Freundlich isotherm model equations. In this study, two classical adsorption models were employed to describe the ion adsorption equilibrium. Langmuir isotherm is valid for monolayer adsorption onto a surface with a finite number of identical sites.

The Langmuir and Freundlich adsorption isotherm model can be expressed as follows:

$$\frac{C_e}{q_e} = \frac{1}{K_d q_m} + \frac{1}{q_m} C_e \quad (3)$$

$$\ln q_e = \ln K_F + \frac{1}{n} \ln C_e \quad (4)$$

where, C_e (mg/L) is the equilibrium concentration of ion in the solution, $q_e$and q_m (mg/g) is the maximum adsorption capacity at equilibrium, and K_d (L/mg) is the effective dissociation constant that relates to affinity binding site, K_F and n are physical constants representing the adsorption capacity and intensity of adsorption respectively.

The slope and intercept of linear Freundlich equation is equal to 1/n and lnK_F respectively. Figure 2 shows the adsorption isotherm of Pb ions onto G-Fe_3O_4 surfaces at 300 K, 310 K and 320 K. From the graph, it can be seen that the adsorption capacity increased with an increase in temperature indicating an endothermic reaction. It is observed that the adsorption percentage increased along with increase of C_e.

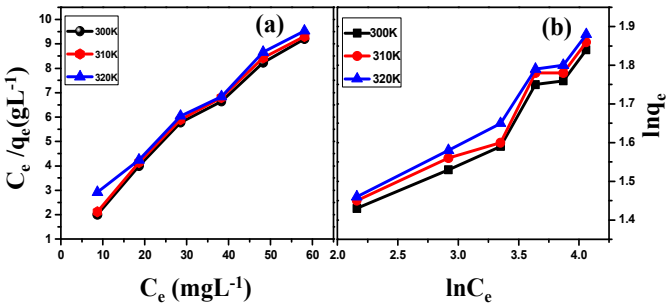

Fig.2. The percentage of adsorption isotherm of Pb ions onto G-Fe_3O_4 surfaces, Initial concentration of ion is 10, 20, 30, 40, 50, and 60 mg/L; pH 5; contact time, 120 min and adsorbent dosage 25 mg/L.

Table 1 Isotherm models for adsorption of Pb ions onto G-Fe_3O_4

Temp(K)	Langmuir			Freundlich		
	K_d	q_m(mg/g)	R^2	K_F	n	R^2
300	0.12	69	0.998	4.2	0.23	0.9328
310	0.1	69	0.992	26.96	0.24	0.9248
320	0.1	67	0.9818	10.86	0.27	0.9686

Two models, Langmuir and Freundlich isotherm model have been adopted for Pb ion adsorption onto G-Fe_3O_4 at different temperatures and at different pH in the experiment. The relative parameters were calculated from the equation and are listed in Table 1. From the R^2 values, the adsorption isotherms can be simulated well by the two models. The table suggests that the adsorption of Pb on G-Fe_3O_4 is mainly as monolayer type.
From the above R^2 values given in Table 1, it can be inferred that Langmuir isotherm fits better into the experimental data than Freundlich isotherm. It was also noted that adsorption is a monolayer process and adsorption of all species requires equal activation energy. From the table it is seen that at different temperature there is a change of q_m and K_d values and the maximum adsorption capacity q_m is obtained as 69 mgg^{-1}.

Thermodynamic Parameters

Thermodynamic parameters provide additional in-depth information regarding the inherent energetic changes involved during adsorption. To assess the thermodynamic parameters, the adsorption isotherm of Pb ions onto G-Fe_3O_4 surfaces were measured at 300, 310 and 320K and the changes in thermodynamic parameters of standard Gibbs free energy of adsorption (ΔG°), standard enthalpy (ΔH°) and standard entropy (ΔS°) were calculated from the variation of the thermodynamic equilibrium constant, K_o, with the change in temperature.

Table 2 Thermodynamics parameters of Pb ion onto G-Fe_3O_4

Temp (K)	ΔG^o	ΔH^o (kJ/mol)	ΔS^o (kJ/mol)
300	-1643		
310	-4796	255.8	15.908
320	-9686		

The standard Gibbs free energy of adsorption, ΔG_o, is

$$\Delta G^o = - RT \ln K_o \quad (5)$$

where R=Gas constant, T =Absolute temperature

$$RT \ln K_o = T \Delta S^o - \Delta H^o \quad (6)$$

From the Table 2, it is clearly seen that the value of change of standard enthalpy is positive and Gibb's free energy is negative showing that the adsorption of Pb ions onto G-Fe_3O_4 adsorbents is endothermic. Consequently, it can be seen that there is a change in the adsorption as temperature increases and here it is seen that adsorption is same at 300 and 310 K.

Table 3 Comparison of adsorption capacities of various adsorbents

Adsorbent	q_m (mg/g)	pH	Ref
CNTs (HNO_3)	35.60	5	32
Granular activated carbon	15.58	5	33
Powdered activated carbon	26.90	5	33
Microbead	16.4	5	34
Iron coated sand	1.21	5	35
G-Fe_3O_4	69	5	Present work

A positive standard enthalpy change suggests that the interaction of Pb ions onto G-Fe_3O_4 is endothermic, which is supported by the increasing adsorption of Pb with increase in temperature. A comparison has been made on the adsorption capacity of various adsorbents cited in the literature towards the removal of Pb ions (Table 3). From the table, it is clearly seen that our G-Fe_3O_4 based adsorbent has the maximum Pb ions adsorption capability.

Photo-Fenton degradation of dye

Further work was carried out on probing the role of the material towards dye degradation applications. Dye adsorption on the catalyst surface is a prerequisite for efficient dye removal. The adsorption of methylene blue dye is studied within 30 min time interval using UV-visible spectroscopy. It can be seen in Fig.S6 that the adsorption of dye is quite rapid in the first 30 min, then gradually rises with increase in adsorption time. After 180 min the amount of dye removed from suspension is calculated using equation given below:

$$\text{Re}\,moval\ (\%) = \frac{1 - C_t}{C_0} X\,100 \quad (7)$$

where C_0 (mg/L) is the initial dye concentration before removal, C_t (mg/L) is the concentration of dye remaining in the solution after stirring for 180 min in dark. The removal efficiency value of composite at different concentration (0.1 to 0.3g/L) and graphene is 49.6, 79.6, 98.5 and 99 %, respectively.

Graphene shows much better removal efficiency in comparison to the composite of same amount (0.2g/L), which can be associated with the large surface area of graphene sheets. Also π–π stacking between dyes and π-conjugation regions of the sheets, can offer more active adsorption sites and catalytic reaction centers.[36]The photocatalytic property of the composite is measured by degradation of dye in the presence of visible light (Fig.3). Before light

irradiation, the suspension of catalyst and dye was stirred for 180 min in the dark in order to reach the adsorption–desorption equilibrium between the catalyst and the dye.It has been observed from Fig. 3 (a & c) that upon addition of H_2O_2 in presence of visible light, degradation rate increases rapidly. For comparison, effect of H_2O_2 in dark on G-Fe_3O_4 composite is also shown in graph (Fig.3b)enlarged view of dye degradation is also shown in Fig. 3 inset. The enhancement in dye degradation can be attributed to the synergistic interaction between GO and Fe_3O_4 nanoparticles. The electron transfer between the NPs and GO sheet facilitates reduction of Fe^{3+} to Fe^{2+} ion. Subsequently, Fe^{2+} would react with H_2O_2 to produce hydroxyl radicals ($OH^{\cdot}$). The hydroxyl radicals produced as a result of Fenton/photo-Fenton processes attacks dye adsorbed on the surface of the catalyst and degrade it to CO_2 and H_2O[37,38].

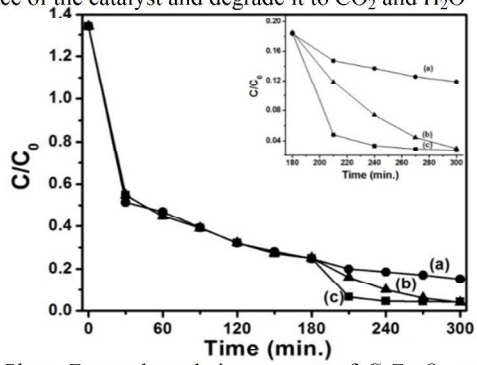

Fig. 3. Photo-Fentondegradation spectra of G-Fe_3O_4 composite at concentration of 0.2g/L in presence of (a) Visible light, (b) H_2O_2 and (c) Visible light and H_2O_2. (Inset shows the expanded view)

For recycling of G-Fe_3O_4 composite the absorbent was separated, washed and then reused. The recycled adsorbed behaviour is shown in Fig. S7. It was observed that the removal efficiency of dye was over 95% upto 5 cycles. The photocatalytic activity of the recycled catalyst was also investigated, and the results are shown in Fig. S7. There is no noticeable change in the photocatalytic activity of the recycled catalyst after five cycles under visible light irradiation, indicating that the magnetically separable photocatalyst is stable and effective for the degradation of organic pollutants in water.

Antibacterial activity of G -Fe_3O_4

Fig.4 shows about 22.66% cells were only viable when treated with G-Fe_3O_4 in comparison to graphene were about 65.33% cells were viable. Two activities were further examined i.e. concentration and time dependent behaviour of G-Fe_3O_4 on E.coli cells. Different concentration of G-Fe_3O_4 (0, 25, 50, 100, 200 ppm) dispersions were incubated with E.coli cells for 60 mins and then plated for examining cell viability. Only E.coli cells and graphene were controls.

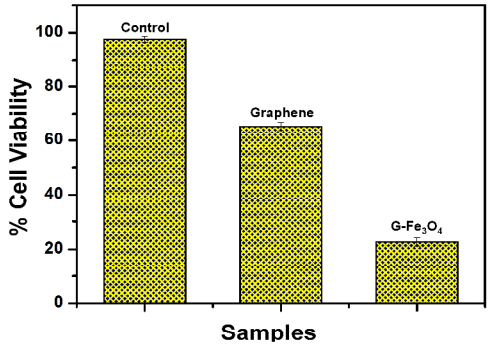

Fig. 4. Cell viability of *E.coli* when treated with graphene and G-Fe_3O_4

It was observed that 25 ppm G-Fe_3O_4 could inhibit 43% cells, as the recorded cell viability as per Fig S8(a) is 57 %. Also 100 ppm was enough to inhibit bacteria as cell viability is 26.84% *E.coli* cells.

On the other hand in time dependent study it was observed that when 100 ppm of G-Fe_3O_4 dispersion was treated with *E.coli* cells for various time intervals from 0 min. to 90 mins, then 60 mins was apt to kill bacteria showing 23.74% cell viability as shown in Fig.S8(b). The loss of *E. coli* viability progressively decreased with the increase of G-Fe_3O_4 concentration. *E. coli* viability has almost decreased from 57% by 25 ppm G-Fe_3O_4 to 21% with 200 ppm. Majority of *E. coli* cells were killed after incubation with G-Fe_3O_4 at a concentration of 100 ppm. In a similar manner, cell viability w.r.t. time from 0-90 mins was drastically decreased from 64.66% to 19.66 % respectively.

Destruction of Bacterial Membrane

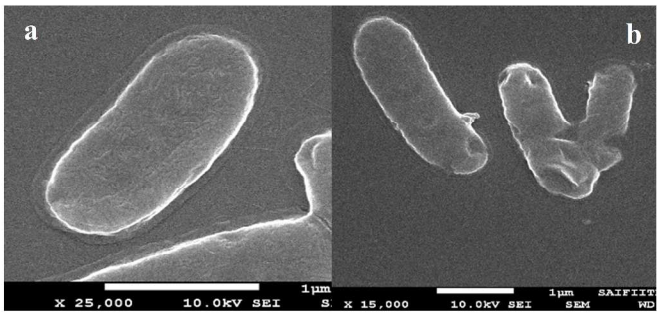

Fig. 5.(a) FE-SEM images of *E.coli* cells control and (b) rapture by G-Fe_3O_4.

FE- SEM was used to illustrate the interaction between G-Fe_3O_4. In Fig. 5 (a) *E.coli* cells as control show entire cell wall without any rupture whereas Fig. 5 (b) has complete disintegration of the cell wall. Spikes created on *E.coli* cells are clear indication that G-Fe_3O_4 has interacted with the cell wall. This kind of cell wall rupture is irreversible damage induced after direct contact with G-Fe_3O_4.

Figure S9 shows the biocompatibility study, and was essential to understand as G-Fe_3O_4 if leached during water purification, so then it should cause no harm to normal cells. As shown, though graphene has less cell compatibility of about 54.11% in 2 mg/ml, whereas at the same concentration, for G-Fe_3O_4 is about 92.99%. Presence of Fe_3O_4 which supposedly has biocompatible nature has been a good support with graphene as biocompatible material.

Biochemical assay of total cellular protein degradation due to effect of G -Fe_3O_4

Degradation of protein due to the effect of graphene and G-Fe_3O_4 was performed by Folin-Lowry test. Table 4 (see in supplementary Information) also indicates reduction in protein content when *E.coli* was treated with graphene and G-Fe_3O_4 individually. The reduction in total protein content was found to be approximately 86.66% in the case of G-Fe_3O_4. Total cellular protein has drastically degraded to 86.66 when treated with G-Fe_3O_4 as observed from table 2, whereas control shows about 236% protein. May be that is why only 22.66% *E.coli* could survive (i.e. 78% mortality) when exposed to 100 ppm G-Fe_3O_4 nanocomposite suggesting that microbial death is due to degradation of total cellular protein.

Total protein assay (by SDS-PAGE methods) of *E.coli* due to effect of G-Fe_3O_4

Fig. 6 depicts degradation of protein analyzed by SDS-PAGE electrophoresis on treating *E.coli* cells with G-Fe_3O_4.It is clear from the protein degradation results that, stress mediated protein degradation of cell membrane left only one higher density protein intact, whereas rest of the proteins were denatured unlike proteins when treated with graphene or control.

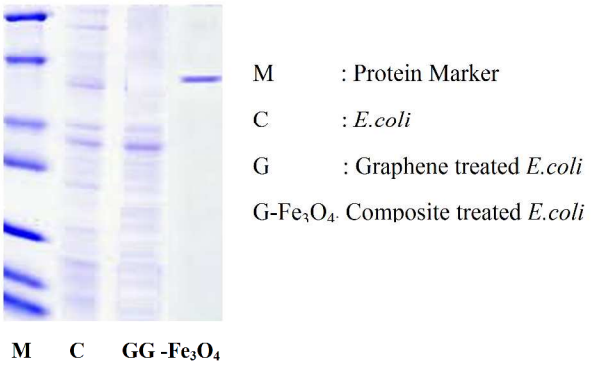

Fig. 6. Protein degradation by G-Fe_3O_4

Glutathione oxidation due to G -Fe_3O_4 treatment

Irregulation of H_2O_2 pathway in the cellular membrane causes oxidative stress. To examine oxidative stress,*in vitro* GSH oxidation was mediated.

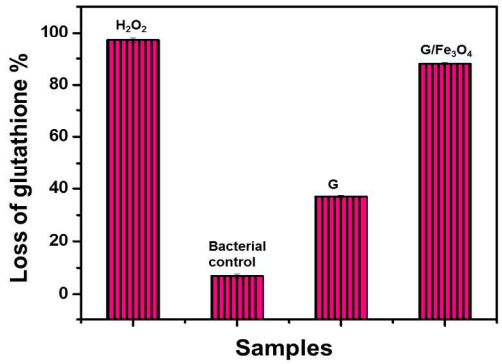

Fig.7. Oxidative stress release by *E.coli* due to effect of G-Fe_3O_4

GSH is a tripeptide with thiol groups. It is an antioxidant in bacteria at a concentration ranging between 0.1 and 10 mM. GSH can prevent damages to cellular components caused by oxidative stress. Thiol groups (-SH) in GSH can be oxidized to disulfide bond (-S-S-), which converts GSH to glutathione disulfide. GSH has been used as an oxidative stress indicator in cells. The Ellman's assay is able to quantify the concentration of thiol groups in GSH. When 0.4mM GSH was incubated with 100 ppm G-Fe_3O_4, the oxidation of GSH gradually advance with extending reaction time upto 60 mins.Fig. 7 shows the fraction of GSH oxidized by G-Fe_3O_4 increases in comparison to graphene. Comparably, G-Fe_3O_4 has significantly higher oxidation reactivity upto89.32% than graphene at the same reaction time and concentration of 60 mins in 125µg/ml of G-Fe_3O_4. The oxidation of GSH indirectly confirms that G-Fe_3O_4 iscapable of mediating ROS-independent oxidative stress toward bacterial cells.

Thus the prepared composite is effective for multipurpose applications due to the combined merits of Fe_3O_4 and graphene.

Conclusions

G-Fe_3O_4 was synthesized by a simple one step solvothermal route from graphene oxide and iron oxide nanoparticles. This nanostructure serves to be an efficient adsorbent for removal of heavy metal ionsfrom waste water. The maximum adsorption capacity of G-Fe_3O_4 was 17 mg/g at initial Pb concentration of 20 mg/L and temperature of 310 K indicating G-Fe_3O_4 is a good adsorbent for the adsorption of Pb (II) ions. The experimental data was well fitted with the Langmuir isotherm model. The monolayer adsorption capacity of Pb by G-Fe_3O_4 was found to be 69 mg/g at 310 K with a pH of 5. Thermodynamic investigations indicated that the adsorption reaction was spontaneous and endothermic. Results indicate that such kind of materials could be used as adsorbents for heavy metal ion removal. Photodegradation of methylene blue dye was successfully achieved upto 5 cycles. Antibacterial activity depicts that 22.33% cells were only viable when treated with G-Fe_3O_4. Further protein degradation confirmed that a higher molecular weight protein was not denatured, whereas rest of the proteins as compared with *E.coli* had disintegrated. This was due to release of some ROS spps. and disintegration of disulphide bond.

Acknowledgements

The author gratefully acknowledges the VIT University, Vellore for supporting this work under the research associate fellowship. Authors acknowledge SAIF and Central surface analytical facility of IIT Bombay

Notes

[a]*Centre for Nanotechnology Research, VIT University, Vellore 632014, India. E-mail: anirmalagladys@gmail.com; anirmalagrace@vit.ac.in;Tel:+919791322311;*

[b]*DST-INSPIRE Faculty, Department of Metallurgical Engineering and Materials Science, Indian Institute of Technology Bombay, Mumbai 400076, India.*

[c] *Department of Metallurgical Engineering and Materials Science, Indian Institute of Technology Bombay, Mumbai, India.*

[d]*Defence Metallurgical Research Laboratory, Hyderabad 500 058, India.*

[e]*Department of Chemistry and Department of Energy Engineering Ulsan National Institute of Science and Technology (UNIST) UNIST-gil 50, Ulsan 689-798, Korea*

References

1 A.K. De, Environmental Chemistry IInd edition, Wiley Eastern Ltd. New Delhi (1992).
2 Sarika Singh,K.C. Barick, D. Bahadur, J. of Hazardous Materials, 2011, **193 (3),**1539–1547.
3 N.A. Babarinde, J.O Babalola, R.A. Sanni,Int. J.Phy. Sci.,2006, **1**, 23-26.
4 A. Saeed, M. Iqbal,M.W. Akhtar, J Hazard Mater B.,2005, **117,** 65–73.
5 T. A. Davis, B. Volesky,A. Mucci, Water Res.,2003, **37,** 4311–4330.
6 G. McKay, Y.S. Ho, Water Res. 1999, **33,** 578–584.
7 B.H. Hameed,A.A. Ahmad,N. Aziz, Desalination. 2009, **247,** 551–560.

8 V.K.Gupta,A. Mittal, R. Jain, M. Mathur,S. Sikarwar, J. Colloid Interface Sci.,2006, **303,** 80–86.
9 Shaobin Liu, Tingying Helen Zeng, Mario Hofmann, Ehdi Burcombe, Jun Wei, Rongrong Jiang, Jing Kong and Yuan Chen, ACS Nano, 2011, **5 (9)**, 6971–6980.
10 Sarika Singh,K.C. Barick, D. Bahadur,, Nanomaterials and Nanotechnology, 2013, 3, 1-19.
11 M.J. Allen, V.C.Tung,R.B. Kaner, Chem. Rev. 2010, **110,** 132–145.
12 M. Ghaedi,A. Hassanzadeh, S.N. Kokhdan, J. Chem. Eng. Data., 2011,**56,** 2511–2520.
13 T.S. Sreeprasad, S.M. Maliyekkal, K.P. Lisha, T. Pradeep, J.Hazard.Mater, 2011, **186**, 921-931.
14 J. Xu, L. Wang, Y. Zhu, Langmuir, 2012, **28**, 8418-8425.
15 S. Gupta, T.S. Sreeprasad, S.M. Maliyekkal, S.K. Das, T. Pradeep, ACS Appl. Mater. Interfaces, 2012, **4**, 4156-4163.
16 S. Wang, H. Sun, H. M. Ang, M.O. Tade, Chem. Eng. J. 2013, **226**, 336-347.
17 M. Machida, T. Mochimaru, H. Tatsumoto, Carbon, 2006, **44**, 2681-2688.
18 R. Zacharia, H. Ulbricht, T. Hertel, Phys. Rev. B., 2004,**69**, 55406.
19 Z. Wu, D. Wang, W. Ren, J. Zhao, G. Zhou,F. Li, H. Cheng, Adv. Funct. Mater., 2010,**20,** 3595–3602.
20 J. Hu, L. Zhong, W. Song, L. Wan, Adv. Mater., 2008,**20**, 2977–2982.
21 Y.M. Zhai, J.F. Zhai, M. Zhou, S.J. Dong, J. Mater. Chem.,2009, **19**, 7030–7035.
22 S. Liu, T. H. Zeng, M. Hofmann, E. Burcombe, J. Wei, R. Jiang, J. Kong, Y. Chen, ACS Nano., 2011, **5**, 6971–6980.
23 W.S. Hummers, R.E. Offeman, J. Am. Chem. Soc., 1958, **80**, 1339.
24 J.P. Ruparelia, S.P. Duttagupta, A.K. Chatterjee, S. Mukherji Desalination,2008, **232,** 145-156.
25 B. Li, Y. Fu, H. Xia, X. Wang, Mat. Letters, 2014, **122**, 193-196.
26 Z.S. Wu, W. Ren, L. Wen, L. Gao, J. Zhao, Z. Chen, G. Zhou, F. Li, H.M. Cheng, ACS Nano, 2010, **4**, 3187-3194.
27 J.K. Lim, S.P. Yeap, H.X. Che, S.C. Low, Nanoscale Res. Lett. 2013, **8**, 381.
28 K.C. Barick, Sarika Singh, M. Aslam, D. Bahadur, Micropor. Mesopor. Mater., 2010, **134**, 195-202.
29 H.Y. Koo, H.J. Lee, H.A. Go, Y.B. Lee, T.S. Bae, J.K. Kim,W.S. Choi, Chem. Eur. J. 2011, **17**, 1214–1219.
30 L. Ren, S. Huang, W. Fan, T. Liu, Appl. Surf. Sci. 2011, **258**, 1132– 1138.
31 T. Liu,Y. Li, Q, Du, J. Sun, Y. Jiao, G. Yang, Z. Wang, Y. Xia, W. Zhang, K. Wang, H. Zhu, D. Wu,Colloids Surf., B., 2012, **90**, 197–203.
32 Y.H.Li, Z.Di, J. Ding, D.Wu, Z. Luan, Y. Zhu, Wat.Res. 2005, **39**, 605-609.
33 Z. Reddad, C. Gerente, Y. Andres, P. Cloirec Le, Environ Sci Technol 2002, **36**, 2067-2073.
34 B. Salih, A. Denizli, C. Kavakli, R. Say, E. Piskin, Talanta, 1998, **77**, 1147-1154.
35 C.H. Lai, C.Y. Chen, Chemosphere, 2001, **44**, 1177-1184.
36 Y.H. Li, S. Wang, Z. Luan, J. Ding, C. Xu, D. Wu, Carbon, 2003, **41**, 1057-1062.
37 S.Q. Liu, B. Xiao, L.R. Feng, S.S. Zhou, Z.G. Chen, Z.Y. Wu, N. Xu, W.C. Oh, Z,D. Meng, Carbon, 2013, **64**, 197-206.
38 S. Guo, G. Zhang, Y. Guo, J.C. Yu, Carbon, 2013, **60**, 437-444.

